

Integration of a UV curable polymer lens and MUMPs structures on a SOI optical bench

Jerwei Hsieh¹, Sheng-Yi Hsiao², Chun-Feng Lai² and Weileun Fang^{2,3}

¹ Instrument Technology Research Center, Hsinchu, Taiwan

² Power Mechanical Engineering, National Tsing Hua University, Hsinchu, Taiwan

³ MEMS Institute, National Tsing Hua University, Hsinchu, Taiwan

E-mail: fang@pme.nthu.edu.tw

Received 17 May 2007, in final form 25 June 2007

Published 30 July 2007

Online at stacks.iop.org/JMM/17/1703

Abstract

This work presents the design concept of integrating a polymer lens, poly-Si MUMPs and single-crystal-silicon HARM structures on a SOI wafer to form a silicon optical bench. This approach enables the monolithic integration of various optical components on the wafer so as to improve the design flexibility of the silicon optical bench. Fabrication processes, including surface and bulk micromachining on the SOI wafer, have been established to realize bi-convex spherical polymer lenses with in-plane as well as out-of-plane optical axes. In addition, a micro device consisting of an in-plane polymer lens, a thick fiber holder and a mechanical shutter driven by an electrothermal actuator is also demonstrated using the present approach. In summary, this study significantly improves the design flexibility as well as the functions of SiOBs.

(Some figures in this article are in colour only in the electronic version)

1. Introduction

The fabrication and integration of micro optical components on a chip to form a silicon optical bench (SiOB) enables various promising applications for MEMS (micro-electro-mechanical-systems). For instance, the applications of SiOBs range from optical communication [1–6], optical storage [7–12], display [13–15] to biotech [16–20], etc. Among the available fabrication techniques, the MUMPs process that uses thin film poly-Si surface micromachining has been extensively employed to fabricate a SiOB [4, 6, 20]. However, the stiffness and moving space of the MUMPs components are usually limited to the thickness of thin films. Meanwhile, optical performance often deteriorates due to the residual stress issues of thin films [4]. On the other hand, single-crystal silicon (SCS) is recognized as a superior material in optical MEMS due to its low intrinsic stress and excellent surface smoothness [5]. Moreover, thick structures, or HARM (high aspect ratio micromachining) structures, are also preferred in some applications to improve the optical performance of the

devices [21]. To this end, micromachining on SOI wafers is gradually increased [2, 5, 12, 14–17]. However, due to the nature of planar fabrication, the flexibility of component design and the variety of available structures are still limited. It is crucial to develop fabrication technologies to improve the flexibility of SiOBs.

Micro lenses can play important roles in many micro optical systems [7–12, 18], and have been realized using various methods [7, 22–26]. Among these, the UV curable polymer micro lens is regarded as a promising material due to its high transmission, low surface roughness and capability to be integrated with other micromachined structures [18]. However, developing a fabrication platform to integrate and align UV curable polymer lenses with various micromachined structures remains a challenge.

Accordingly, this work has established a process to realize a novel SiOB consisting of a UV curable polymer lens, thin film poly-Si components (MUMPs process) and HARM structures (SOI process). The thin film process and SOI process provide the components with the capability of

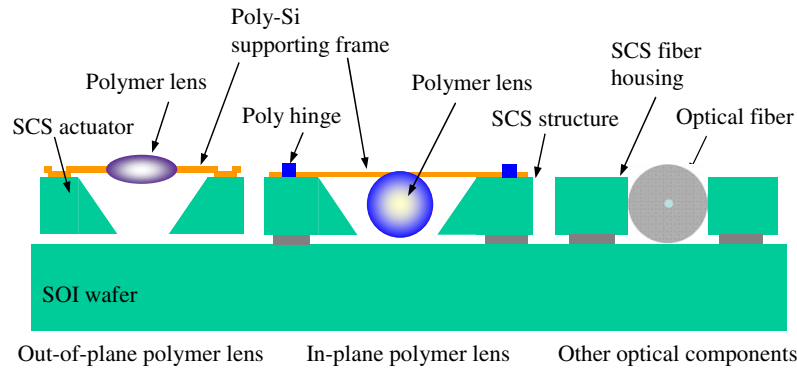


Figure 1. The design concept of the present study to integrate a polymer lens, surface micromachined thin film poly-Si and HARM structures on a SOI wafer to form a SiOB.

moving in the out-of-plan and in-plane directions, respectively. The UV curable polymer process enables the integration of a bi-convex spherical lens on the SiOB. Different optical characteristics of the lenses can be realized by designing different sizes of lens-holding structures as well as the volume of the polymer. As a result, a SiOB with both in-plan and out-of-plan optical paths can be achieved, and the design flexibility as well as the functions of the SiOB can be significantly improved.

2. Concepts and design

Figure 1 shows the design concept of integrating a polymer, surface micromachined thin film poly-Si (MUMPs) and HARM structures on a SOI wafer to form a silicon optical bench. In general, a single poly-Si thin film which anchors to the SOI wafer can be exploited as the supporting frame for the polymer lens with focal point in the out-of-plane direction (named the out-of-plane polymer lens). In addition, the two poly-Si thin film structures can be employed to implement not only the supporting frame for the polymer lens but also the hinges to allow angular motion of the frame and lens, as indicated in figure 1. Therefore, angular motion of the supporting frame can be achieved, which enables the polymer lens with its optical axis in the in-plane direction (named the in-plane polymer lens). This study further exploits the device layer of the SOI wafer to realize various HARM structures, for instance, the thick fiber housing of good clamping ability, and the SCS actuator with larger output force and displacement. Detailed information regarding the fabrication and integration of the components in figure 1 will be presented in section 3, whereas the design considerations of the formation of a polymer lens and the assembly of the in-plane polymer lens are discussed as follows.

2.1. Polymer lens

According to different applications, various materials have been employed to implement a micro lens. In this study, the UV curable polymer is exploited as lens material. As shown in figure 2, a circular supporting frame made of poly-Si with a given diameter and thickness is first provided. The liquid type UV polymer is then dropped onto the supporting

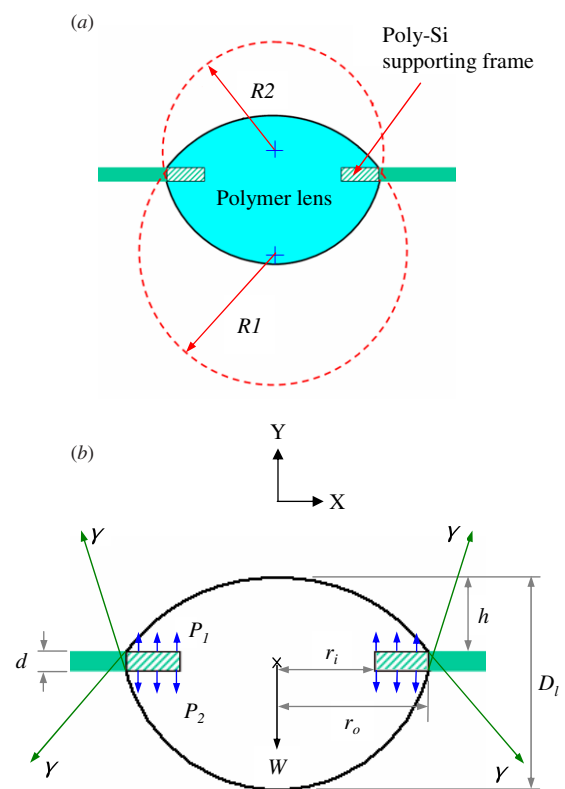


Figure 2. (a) Schematic drawing of the bi-convex micro lens formed by the UV curable polymer and (b) the forces applied on the polymer lens before curing.

frame. Because of the cohesion and surface tension of the liquid polymer, the UV polymer forms a bi-convex spherical lens. Due to the effect of gravity G , the radius of curvature R_1 (for the upper surface) and the radius of curvature R_2 (for the lower surface) are different, as indicated in figure 2(a). The volume V of the bi-convex lens is derived as

$$V = \frac{-2\pi}{3} [(R_1^2 - r_o^2)^{\frac{3}{2}} + (R_2^2 - r_o^2)^{\frac{3}{2}} - R_1^3 - R_2^3] + \pi d r_i^2 \tag{1}$$

where d is the thickness of the supporting frame, and r_i and r_o are the inner and outer frame radii, respectively. Considering

the polymer material of density ρ and surface tension γ , the forces exerted on the lens in the vertical direction consist of the gravity force W , the surface tension force S and the reaction force N . The force W can be expressed as

$$W = V\rho G. \quad (2)$$

The force S can be obtained from the vertical component of surface tension force at the air–liquid interface,

$$S = 2\pi r_o^2 \left(\frac{1}{R_2} - \frac{1}{R_1} \right) \gamma. \quad (3)$$

In addition, the force N is derived from the net force induced by the liquid pressure P_1 and P_2 at the solid–liquid interface,

$$N = (\rho Gh - \rho G(h + d)) \times (2\pi r_o^2 - 2\pi r_i^2) \quad (4)$$

where h is the height of the upper lens depicted in figure 2(b). Considering the force balance in the vertical (out-of-plane) direction, the equation of equilibrium can be expressed as

$$W = N + S. \quad (5)$$

As a result, the lens volume V can be further obtained as

$$V = \frac{1}{\rho G} 2\pi r_o^2 \left(\frac{1}{R_2} - \frac{1}{R_1} \right) \gamma - 2\pi d(r_o^2 - r_i^2). \quad (6)$$

In this study, the dimensions r_o , r_i and d of the supporting frame, and the material properties ρ , and γ of the polymer are prescribed design parameters. Thus, the lens curvatures R_1 and R_2 can be predicted by equations (1) and (6) for a given polymer volume V . In other words, the optical characteristic of the bi-convex lens can be tuned by varying the polymer volume during the process. The focal length f of the present bi-convex lens can thus be determined as

$$f = \frac{1}{(n-1) \left[\frac{1}{R_2} - \frac{1}{R_1} + \frac{D_l}{R_1 R_2} \frac{n-1}{n} \right]} \quad (7)$$

where n and D_l are the refractive index and center thickness of the polymer lens in figure 2(b), respectively.

2.2. Assembly of an in-plane polymer lens

As shown in figure 1, the out-of-plane polymer lens integrated with the single crystal silicon structures can easily be realized by dropping a UV curable polymer onto the supporting frame and then solidifying it by UV light curing. Due to the nature of planar micromachining, however, it is hard to directly realize an in-plane polymer lens. Accordingly, various post-assembling methods, such as reflowing PR [27] and assembled by micro actuators [7, 28], have been developed. To prevent the complexity, this study proposes a novel assembly method that uses the self-weight of lens as the assembly force, which concept is illustrated in figure 3. Before the final step of removing the sacrificial layer, the UV curable polymer is dropped onto the poly-Si supporting frame. In this study, the center of the lens supporting frame is designed to have an offset from the axis AA' , as shown in figure 3(a). As a result, a moment on the axis AA' will be provided by the weight of the polymer lens, and is balanced by the constraint of the sacrificial layer. After the polymer lens is solidified by UV curing, the sacrificial layer is etched away and the poly-Si frame structures become freely to move, causing the polymer lens and supporting frame rotate about the hinge spontaneously. Finally, the in-plane polymer lens can be implemented, as shown in figure 3(b). More precise alignment can be achieved by designing some wedge-shaped positioner at the rotating axis of the supporting frame.

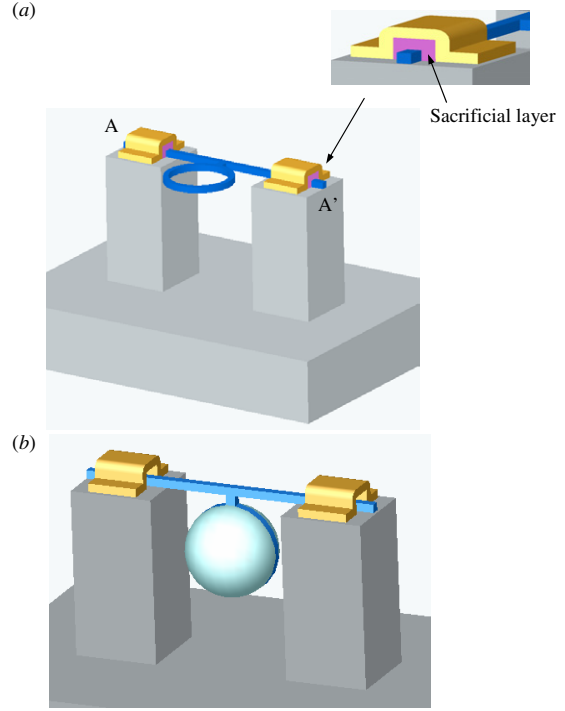


Figure 3. The present concept to realize the in-plane polymer lens: (a) before removing the sacrificial layer and (b) positioning of the polymer lens in the in-plane direction by its self-weight after removing the sacrificial layer.

3. Fabrication and results

To realize the proposed design, a process integrating surface- and bulk- micro machining on a SOI wafer has been developed in this work. The present processes begin with the two poly-Si surface micromachining on a SOI substrate, as illustrated in figure 4(a). Thermal and PECVD oxide films are used as the sacrificial layers, while the first and second poly-Si layers are employed to form the supporting frame and hinges, respectively. After patterning the sacrificial and structure layers, a LPCVD nitride film is deposited and patterned to protect these thin film layers, as shown in figure 4(b). TMAH solution is then used to anisotropically etch away the SCS material beneath the frame structure, as shown in figure 4(c). Through this undercutting step moving space for the lens can be provided. During TMAH etching, the poly-Si layers which fully covered by the oxide and nitride films are properly protected. As shown in figure 4(d), a DRIE process is subsequently used to etch the device layer of the SOI wafer. The required high-aspect-ratio silicon structures, such as fiber housing and micro actuators, are thus realized. The poly-Si layers are then partially released after time-etching of the sacrificial oxide layers, as shown in figure 4(e). Proper design of hinge length is required to guarantee a portion of the sacrificial oxide inside the poly-Si hinge not being removed. As a result, the poly-Si frame structure remains in its original position. Meanwhile, the insulation layer of the SOI wafer is also partially removed during the BOE etching. As shown in figure 4(f), the commercial UV curable polymer NOA63 is then dropped onto the poly-Si frame and solidified by

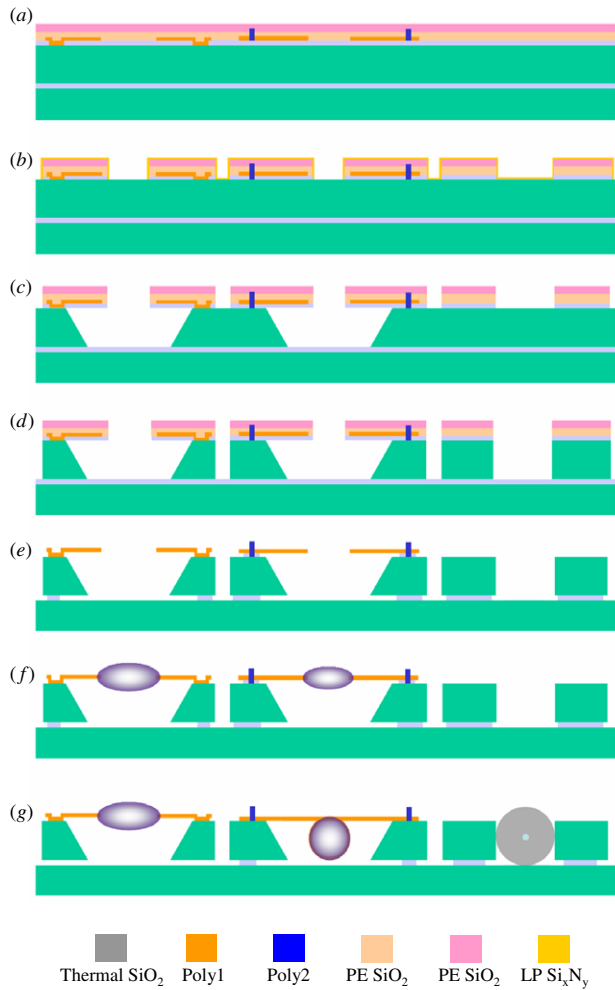


Figure 4. Process flow of the integrated fabrication process.

UV light curing. The volume of the polymer is controlled pneumatically by commercial dispensing equipment. Finally, the wafer is immersed into BOE again to fully remove the sacrificial oxide. Within a proper etching time, the polymer lens could remain intact. Upon releasing the sacrificial oxide, the polymer lens and supporting frame rotate about the hinge spontaneously, as shown in figure 4(g). Finally, the in-plane polymer lens is implemented and aligned well to the in-plane optical components such as optical fiber housing and vertical mirrors. The lens and supporting frame can be fixed at their positions by an extra polymer dropping/solidifying process.

Using the process described above, various devices have been successfully fabricated and integrated on the SOI wafer. The SEM photos in figure 5 show the integration of the out-of-plane polymer lens with a linear movable stage. As indicated in figure 5(a), a 2 μm thick lens supporting frame consisting of a circular-ring and two beams are anchored on a movable stage. The movable stage consisting of a supporting frame and an actuator are made of 100 μm thick device silicon layer. It is remarkable that the device layer under the poly-Si was successfully removed by the process presented in figure 4. Figure 5(b) shows the device after the formation of a bi-convex polymer lens. The measured radius of curvature of the upper

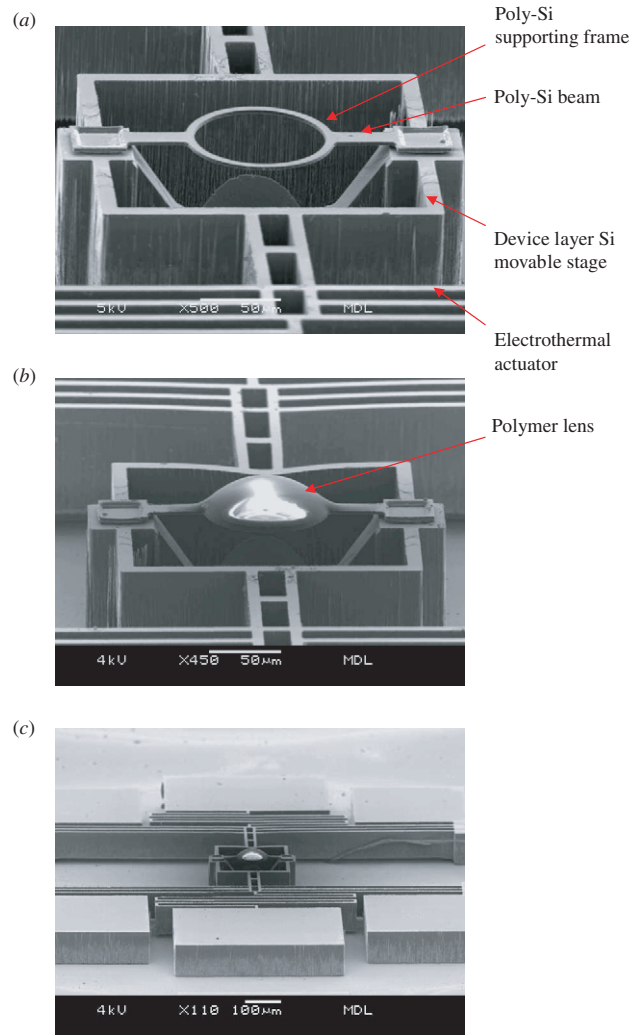


Figure 5. SEM photos of the out-of-plane polymer lens and its integration with a linear moving stage: (a) poly-Si supporting frame without polymer lens, (b) poly-Si supporting frame with polymer lens and (c) the whole device.

lens surface is different from that of the lower lens surface, as expected. Figure 5(c) shows a bird's-eye view of the device, where the whole device including the electrothermal actuators and bond pads can be observed. The photos in figure 6 show the formation of an in-plane polymer lens. Six poly-Si hinges are anchored on the 100 μm thick supporting posts made of the device layer of a SOI wafer. The hinges are used to confine the motion of the 2 μm thick poly-Si lens supporting frame, as shown in figure 6(a). The material underneath the poly-Si was fully removed to offer a large moving space for the polymer lens. Figure 6(b) shows the device after the formation of a bi-convex polymer lens. The sacrificial layer between the poly-Si lens supporting frame and hinges was not removed yet. Thus, the polymer lens in figure 6(b) remained in the out-of-plane direction. After completely removing the sacrificial layer underneath the hinges, the polymer lens and the poly-Si lens supporting frame rotated about the hinges due to the self-weight of the lens. Figure 6(c) shows that the polymer lens successfully rotated to the in-plane direction

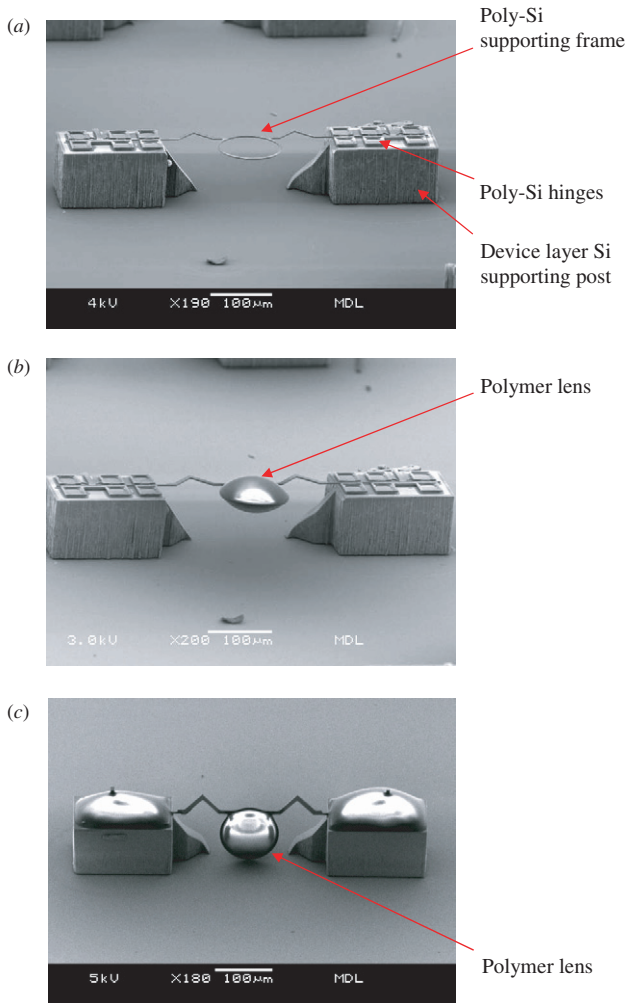


Figure 6. Fabrication results of the in-plane polymer lens. Before removing the sacrificial layer: (a) poly-Si supporting frame, (b) poly-Si supporting frame with an out-of-plane polymer lens, and after removing the sacrificial layer (c) poly-Si supporting frame with an in-plane polymer lens.

after the sacrificial layer being etched away, and further fixed by the UV curable polymer. The SEM photo in figure 7 demonstrates the integration of the in-plane polymer lens with a thick fiber housing and a mechanical shutter driven by an electrothermal actuator. The polymer lens along with the poly-Si supporting frame has been fixed at the final position by the UV curable polymer. The fiber housing, shutter and electrothermal actuator were easily implemented using the device layer of the SOI wafer. Moreover, the positions of the fiber housing and the lens were defined by photo lithography. As a result, the optical components in figure 7 are precisely integrated and aligned to form the present SiOB on a SOI wafer.

4. Lens characterization and testing

The performances of the devices in figures 5–7 have been characterized to demonstrate the feasibility of the present study. First, a commercial white light interferometer has been

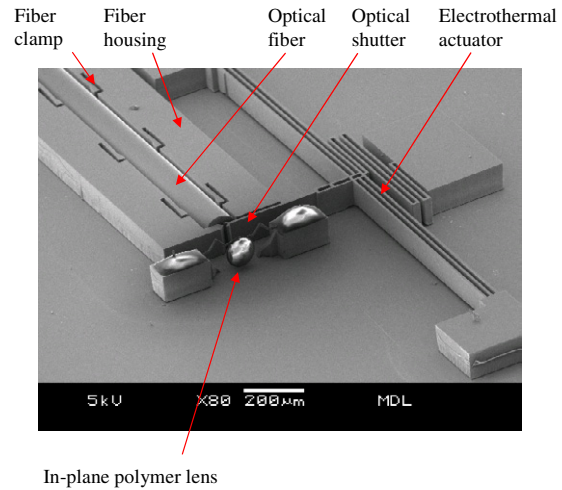


Figure 7. SEM photo of an in-plane polymer lens integrating with a thick fiber housing, and a optical shutter driven by an electrothermal actuator. The lens and poly-Si frame has been fixed by UV curable polymer on the hinge area. An optical fiber has been aligned and clamped in the fiber housing.

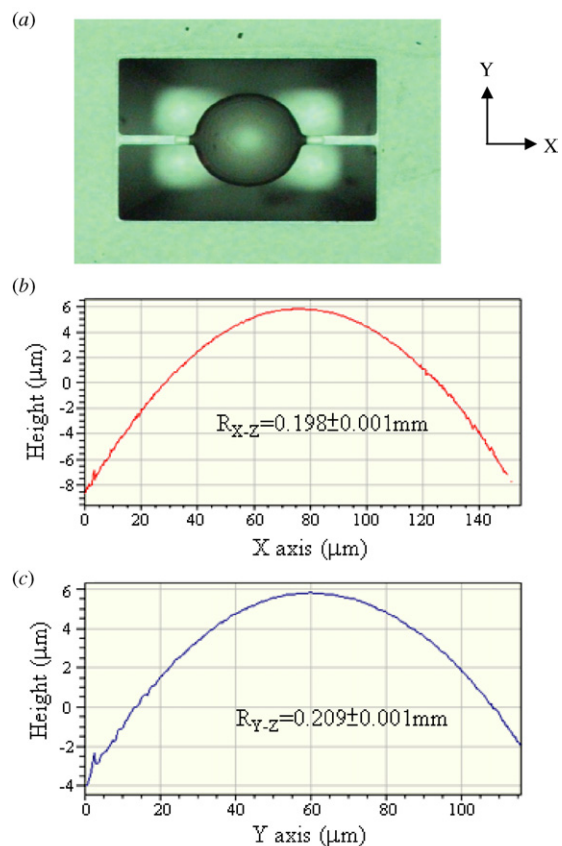


Figure 8. The typical measured surface profiles (by a WYKO interferometer) of the polymer lens: (a) top-view photo of the polymer lens, (b) the lens surface profile in X–Z cross section and (c) the lens surface profile in Y–Z cross section.

employed to measure the surface profile of the polymer lens. The typical measurement results on the radius of curvature and the surface roughness of the lens shown in figure 8(a) are

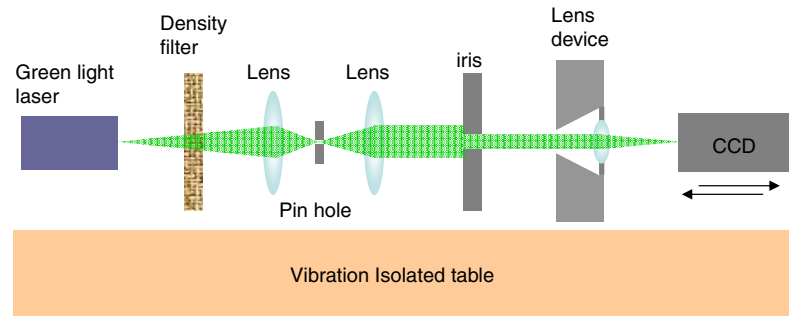


Figure 9. The test setup to measure the focal length of the polymer lens.

shown in figures 8(b) and (c). The lens surface profiles along the X -axis and Y -axis respectively are also obtained. In this case, the polymer lens has a measured radius of curvatures R_1 (for upper surface) of 0.198 ± 0.001 mm. It is noted that R_1 on the X - Z cross section is slightly increased to 0.209 ± 0.001 mm owing to the existence of the beams (in X -axis) attached to the supporting frame. It was speculated that a small amount of the polymer was flowed to the beams before the material being cured, causing the lens slightly unsymmetrical for the X -axis and Y -axis. Nevertheless, the assumption of a spherical polymer lens in section 2 is acceptable. The average radius of curvatures R_1 for ten different polymer lenses is 0.196 mm with a standard deviation of 2.11%. This study also measured the radius of curvatures R_2 for three different lenses. The measured R_2 and their associated R_1 are 0.357 mm ($R_1 = 0.362$ mm), 0.323 mm ($R_1 = 0.337$ mm) and 0.331 mm ($R_1 = 0.349$ mm). As a comparison, the radius of curvatures R_2 predicted by the method depicted in section 2.1 are 0.357 mm, 0.333 mm and 0.344 mm. Thus, the maximal deviation between the analysis and experiment results is below 3.9%. In addition, the typical surface roughness R_{rms} of the polymer lens was about 10 nm; thus a small scattering loss can be guaranteed.

The test setup in figure 9 was established to measure the focal length of the polymer lens. The pin hole and iris were employed to provide collimated light with an adequate beam diameter. The focal length is determined by the distance between the polymer lens and CCD when a minimal diameter of beam spot was observed by the CCD. The measurement error of focal length, mainly resulting from the slightly misjudgment of the minimum beam spot as well as the finite resolution of the moving stage, is about ± 0.005 mm. The photos in figure 10 show the beam images captured by the CCD camera. As shown in figures 10(a)–(c), the beam diameter decreases when the CCD moves away from the polymer lens. The minimal diameter of the beam spot can be observed while the CCD focal plane is coincident with the focal plane of the polymer lens, as shown in figure 10(c). As a result, the lens with $R_1 = 0.349$ mm and $R_2 = 0.331$ mm has the measured focal length of 0.307 mm and numerical aperture (NA) of 0.38. Using a refractive index of 1.56 and a lens thickness of 0.065 mm, the focal length calculated from equation (7) is 0.314 mm. The deviation of

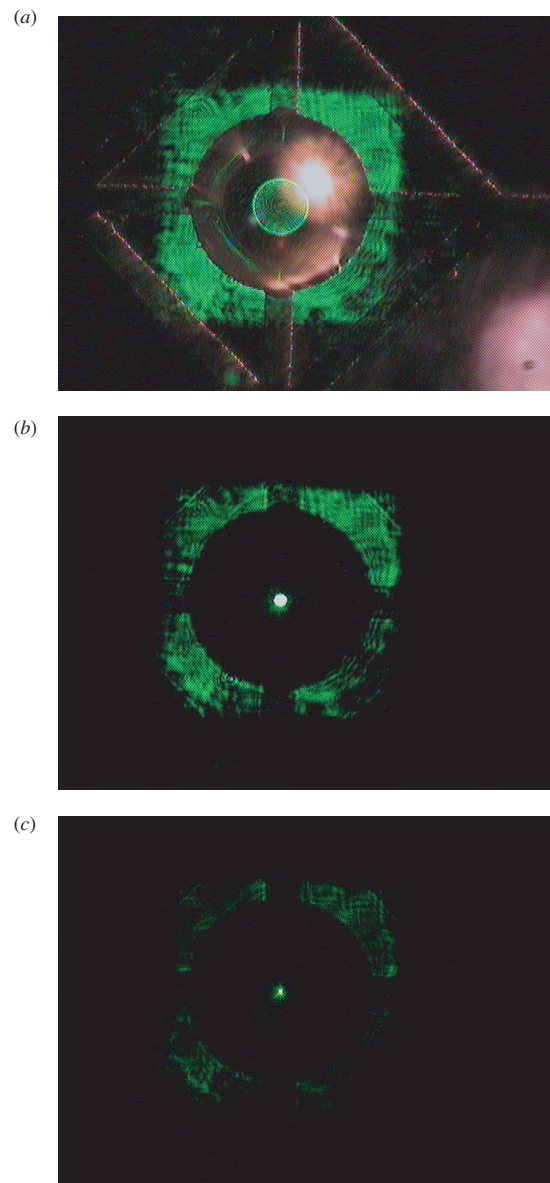


Figure 10. Images of the laser beam spot captured at different positions of the CCD.

2.3% reveals good agreement on calculation and experimental results.

5. Conclusions

This work successfully demonstrates the fabrication and integration of thin-film MUMPs, thick HARM and polymer structures on a SOI wafer to form a SiOB. Various components which can move in either in-plane or out-of-plane direction can be fabricated and integrated using the present approach. In applications, a bi-convex spherical polymer lens positioned in both in-plane and out-of-plane directions has been successfully fabricated. A model to predict the profiles of a polymer lens has also been established and experimentally verified. The focal length of the lens can be controlled by the volume of the polymer, which is determined by commercial dispensing equipment. The measurement results indicate that the bi-convex spherical polymer lens has a typical focal length of 0.307 mm and a numerical aperture of 0.38. The out-of-plane-direction polymer lenses integrated with a poly-Si frame supported by a stationary or movable stage are demonstrated. In addition, a micro device consisting of an in-plane-direction polymer lens, thick fiber housing, and a mechanical shutter driven by an electrothermal actuator is also realized. In summary, the design flexibility as well as the functions of the SiOB can be significantly expanded.

Acknowledgments

This paper was (partially) supported by the Ministry of Economic Affairs, Taiwan, under contract no. 95-EC-17-A-07-S1-0011 and by the Nation Science Council, Taiwan, under contract NSC 94-2212-E-007-026. The authors would also like to thank the Center for Nano-Science and Technology in the Tsing Hua University (Taiwan), the Nano Facility Center of National Chiao Tung University (Taiwan) and the NSC National Nano Device Laboratory (Taiwan) for providing the fabrication facilities.

References

- [1] Toshiyoshi H and Fujita H 1996 Electrostatic micro torsion mirrors for an optical switch matrix *J. Microelectromech. Syst.* **5** 231–7
- [2] Isamoto K, Kato K, Morosawa A, Chong C, Fujita H and Toshiyoshi H 2004 A 5-V operated MEMS variable optical attenuator by SOI bulk micromachining *IEEE J. Sel. Top. Quantum Electron.* **10** 570–8
- [3] Fan L *et al* 2002 Digital MEMS switch for planar photonic crossconnects *OFC—Postconference Tech. Dig. (Washington, DC)* vol 1, pp 93–4
- [4] Lin L-Y, Goldstein E L and Tkach R W 2000 On the expandability of free-space micromachined optical cross connect *J. Lightwave Technol.* **18** 482–9
- [5] Greywall D S, Busch P A, Pardo F, Carr D W, Bogart G and Soh H T 2003 Crystalline silicon tilting mirrors for optical cross-connect switches *J. Microelectromech. Syst.* **12** 708–12
- [6] Toshiyoshi H, Su G-D J, LaCosse J and Wu M C 2003 A surface micromachined optical scanner array using photoresist lenses fabricated by a thermal reflow process *J. Lightwave Technol.* **21** 1700–8
- [7] Ming C Wu 1997 Micromachining for optical and optoelectronic systems *Proc. IEEE* vol 85, pp 1833–56
- [8] Wu M, Hsiao S-Y, Peng C-Y and Fang W 2006 Development of tracking and focusing micro actuators for dual-stage optical pick-up head *J. Opt. A: Pure Appl. Opt.* **8** s323–9
- [9] Kim S-H, Yee Y, Choi J, Kwon H, Ha M-H, Oh C and Bu J U 2004 A micro optical flying head for a PCMCIA-sized optical data storage *Tech. Dig. IEEE Int. Conf. MEMS (Maastricht, The Netherlands, Jan. 25–29)* pp 85–8
- [10] Hata S, Yamada Y, Ichihara J and Shimokohbe A 2002 A micro lens actuator for optical flying head *Tech. Dig. IEEE Int. Conf. MEMS (Las Vegas, NV, Jan. 20–24)* pp 507–10
- [11] Blankenbeckler D L, Bell B W Jr, Ramadurai K and Mahajan R L 2006 Recent advancements in datatray's small form-factor optical disc and drive *Japan. J. Appl. Phys.* **45**
- [12] Cheng H-D, Hsiao S-Y, Wu M and Fang W 2007 Integrated tracking and focusing systems of MEMS optical pickup head *IEEE Trans. Magn.* **43** 805–7
- [13] Muller R S and Lau K Y 1998 Surface-micromachined microoptical elements and systems *Proc. IEEE* vol 86, pp 1705–20
- [14] Ko Y-C *et al* 2006 Gimbaled 2D scanning mirror with vertical combs for laser display *Proc. IEEE/LEOS Int. Conf. Opt. MEMS (Big Sky, MT, Aug. 21–24)* pp 104–5
- [15] Yalcinkaya A D, Urey H, Brown D, Montague T and Sprague R 2006 Two-axis electromagnetic microscanner for high resolution displays *J. Microelectromech. Syst.* **15** 786–94
- [16] Hsieh J, Hsiao S-Y, Yin H-L, Chen W-C, Weng C-J, Lin Y-H, Fang W and Shieh K-W 2005 An in-plane dispersive system utilizing micro tunable vertical grating *Proc. IEEE/LEOS Int. Conf. Opt. MEMS (Oulu, Finland, Aug. 1–4)* pp 97–8
- [17] Nakada M, Chong C, Isamoto K, Fujita H and Toshiyoshi H 2006 Design and fabrication of optical MEMS scanners *Proc. IEEE/LEOS Int. Conf. Opt. MEMS (Big Sky, MT, Aug. 21–24)* pp 34–5
- [18] Kwon S and Lee L P 2002 Stacked two dimensional micro-lens scanner for micro confocal imaging array *Tech. Dig. IEEE Int. Conf. MEMS (Las Vegas, NV, Jan. 20–24)* pp 483–6
- [19] Yu K, Lee D, Krishnamoorthy U, Park N and Solgaard O 2006 Micromachined fourier transform spectrometer on silicon optical bench platform *Sensors Actuators A* **130–131** 523–30
- [20] Kiang M-H, Nee J T, Lau K Y and Muller R S 1997 Surface-micromachined diffraction gratings for scanning spectroscopic applications *Proc. Int. Conf. Solid-State Sens. and Actuators (Transducers) (Chicago, IL, Jun. 16–19)* vol 1, pp 343–5
- [21] Chu P B, Lee S-S, Park S, Tsai M J, Brener I, Peale D, Doran R A and Pu C 2001 MOEMS-enabling technologies for large optical cross-connects *Proc. SPIE* **4561** 55–65
- [22] Heremans P, Genoe J, Kuijk M, Vounckx R and Borghs G 1997 Mushroom microlenses: optimized microlenses by reflow of multiple layers of photoresist *IEEE Photon. Lett.* **9** 1367–9
- [23] Shimada J, Ohguchi O and Sawada R 1991 Microlens fabricated by the planar process *J. Lightwave Technol.* **9** 571–6
- [24] Lee S-K, Lee K-C and Lee S S 2002 Microlens fabrication by the modified LIGA process *Tech. Dig. IEEE Int. Conf. MEMS (Las Vegas, NV, Jan. 20–24)* pp 544–7
- [25] Hsieh J, Weng C-J, Yin H-L, Lin H-H and Chou H-Y 2005 Realization and characterization of SU-8 micro cylindrical lenses for in-plane micro optical systems *Microsyst. Technol. J.* **11** 429–37
- [26] MacFarlane D L, Narayan V, Tatum J A, Cox W R, Chen T and Hayes D J 1994 Microjet fabrication of microlens arrays *IEEE Photon. Technol. Lett.* **6** 1112–4
- [27] Syms R R A 2000 Refractive collimating microlens arrays by surface tension self-assembly *IEEE Photon. Technol. Lett.* **12** 1507–9
- [28] Lin L Y, Shen J L, Lee S S and Wu M C 1997 Surface-micromachined micro-XYZ stages for free-space microoptical bench *IEEE Photon. Technol. Lett.* **9** 345–7